PAPER • OPEN ACCESS

Clamped seismic metamaterials: ultra-low frequency stop bands

New Journal of Physics
The open access journal at the forefront of physics

Deutsche Physikalische Gesellschaft DPG
IOP Institute of Physics

Published in partnership with: Deutsche Physikalische Gesellschaft and the Institute of Physics

OPEN ACCESS

RECEIVED
22 January 2017

REVISED
28 March 2017

ACCEPTED FOR PUBLICATION
20 April 2017

PUBLISHED
16 June 2017

PAPER

Clamped seismic metamaterials: ultra-low frequency stop bands

Y Achaoui[1], T Antonakakis[2], S Brûlé[3], R V Craster[4,5], S Enoch[1] and S Guenneau[1]

[1] Aix Marseille Univ, CNRS, Centrale Marseille, Institut Fresnel, Marseille, France
[2] Multiwave Technologies AG, 3 Chemin du Pré Fleuri 1228, Geneva, Switzerland
[3] Dynamic Soil Laboratory, Ménard, F-91620 Nozay, France
[4] Department of Mathematics, Imperial College London, London SW7 2AZ, United Kingdom
[5] Author to whom any correspondence should be addressed

E-mail: r.craster@imperial.ac.uk

Keywords: phononic crystal, mechanical metamaterial, seismic waves

Supplementary material for this article is available online

Abstract

The regularity of earthquakes, their destructive power, and the nuisance of ground vibration in urban environments, all motivate designs of defence structures to lessen the impact of seismic and ground vibration waves on buildings. Low frequency waves, in the range 1–10 Hz for earthquakes and up to a few tens of Hz for vibrations generated by human activities, cause a large amount of damage, or inconvenience; depending on the geological conditions they can travel considerable distances and may match the resonant fundamental frequency of buildings. The ultimate aim of any seismic metamaterial, or any other seismic shield, is to protect over this entire range of frequencies; the long wavelengths involved, and low frequency, have meant this has been unachievable to date. Notably this is scalable and the effects also hold for smaller devices in ultrasonics. There are three approaches to obtaining shielding effects: bragg scattering, locally resonant sub-wavelength inclusions and zero-frequency stop-band media. The former two have been explored, but the latter has not and is examined here. Elastic flexural waves, applicable in the mechanical vibrations of thin elastic plates, can be designed to have a broad zero-frequency stop-band using a periodic array of very small clamped circles. Inspired by this experimental and theoretical observation, all be it in a situation far removed from seismic waves, we demonstrate that it is possible to achieve elastic surface (Rayleigh) wave reflectors at very large wavelengths in structured soils modelled as a fully elastic layer periodically clamped to bedrock. We identify zero frequency stop-bands that only exist in the limit of columns of concrete clamped at their base to the bedrock. In a realistic configuration of a sedimentary basin 15 m deep we observe a zero frequency stop-band covering a broad frequency range of 0–30 Hz.

1. Introduction

The desire to deflect, absorb or redirect waves is ubiquitous across many fields: electromagnetics, optics, hydrodynamics, acoustics and elasticity. Various techniques have been developed, often in one field but not in the others, and we are going to draw upon advances in optics and electromagnetic wave systems to develop a methodology for reflecting long-wavelength seismic waves in sedimentary basins. The motivations to do so are clear: according to the US Geological Survey there are millions of earthquakes every year worldwide, the vast majority are magnitude 3.9 or lower but more than 1000 measure 5.0 or higher on the Richter scale [1]. Ground vibrations, caused by even minor earthquakes, have an impact upon the structural integrity of buildings and similarly intrusive ground vibrations from urban train systems, subways, machinery such as piledrivers and roads often affect property values or land usage. These vibrations are not simply a nuisance, but small magnitude vibration due to machinery, or nearby railway lines, can cause significant damage to buildings, especially over time [2]. Furthermore, for buildings such as nuclear power plants and oil refineries, even a small level of damage can have disastrous consequences. Seismic waves consist of surface waves (elliptically polarized Rayleigh waves

and horizontally polarized Love waves), pressure bulk waves and shear bulk waves; surface waves cause the majority of any damage and travel farthest, but bulk pressure, and shear, waves also cause damage, especially where wave trapping occurs in sedimentary basins (so-called seismic site effects). Designing a defence structure to prevent seismic waves from reaching buildings is therefore of substantial interest particularly for long waves with frequency in the range 1–10Hz as this corresponds to the resonant fundamental frequency of many man-made structures [3]. It is, of course, these long, low frequency, waves that are the hardest to develop protection measures against and it is an open problem to develop such devices.

Since the late 1980s, in optics, researchers have taken advantage of technological improvements in structuring matter to achieve control over the flow of light [4, 5]. The photonic crystals typically used are periodic man-made structures that inhibit emission due to band gaps [6, 7], i.e., ranges of frequency in which light cannot propagate through the structure. The existence of stop-bands is well predicted by Floquet–Bloch theory, which can be applied to any type of waves propagating within periodic media [8–10]. Importantly, for practical implementation, periodicity need not be perfect to preserve existence of stop-bands [11]. For such periodic structures, striking effects such as slow light can be achieved on edges of stop-bands where the wave group velocity vanishes [12]. More recently the field of metamaterials has emerged that uses periodic arrangements of elements with size much smaller than the considered wavelength (typically hundreds of nanometers) that acquire effective properties of materials with negative optical index [13, 14], or highly anisotropic materials such as hyperbolic metamaterials [15] or can be used to create invisibility cloaking devices [16, 17].

These ideas have been translated to acoustics and the corresponding acoustic phononic crystals have had success with early work by Sigalas and Economou [18] showing that an infinite 2D array of high-density parallel cylinders embedded in a low-density host material possesses a complete band gap in two-dimensions; these effects are beautifully illustrated by the sound attenuation through a sculpture by artist Eusebio Sempere [19], that exhibits partial stop-bands from 1.5 to 4.5 kHz, which has had impact both on the scientific community and the general public. Aside from acoustics, these ideas have had applications in other wave systems such as proposed breakwater devices, Hu and Chan [20], for surface ocean waves as a potential application of photonic crystals at the meter-scale. In the same spirit, some of us envisioned rerouting ocean waves around a region of still water surrounded by concentric arrays of pillars [21]; non-overtopping dykes for ocean waves can be also envisaged with meter scale invisibility carpets for water waves [22, 23].

Elastic phononic crystals can also be envisaged and typically fall into studies of flexural thin elastic plates, bulk media or surface waves atop thick elastic substrates; the latter supporting Rayleigh surface waves. There are close analogies with electromagnetic surface waves, as an example, surface plasmons, which have features close to those of Rayleigh waves at least qualitatively. Reference [24] showed the existence of Rayleigh–Bloch waves in linear periodic gratings for flexural waves and these also appear in the full elastodynamic setting [25]. These Rayleigh–Bloch waves are elastic waves localised to the grating, exponentially decaying away from the grating, and only exist due to the periodicity, these have direct parallels to spoof plasmons in the field of plasmonics, which is devoted to the control of surface electromagnetic waves in structured metals [26, 27]. Thus at least qualitatively ideas from electromagnetism transfer to the elastic cases and can act as strong motivation.

This activity has motivated experiments on the control of surface acoustic waves on the microscale in phononic crystals, with holes, that have been performed by Benchabane *et al* [28] and extended to the hypersonic regime [29]. Protrusions such as pillars atop an elastic substrate have also been considered [30, 31] inspiring studies using negative refraction for Rayleigh [32] and Lamb [33–35] waves. Such interactions between resonators on the surface, or surface defects, and surface waves have found widespread application in phononic membranes [36] and in interrogating the contact adhesion of microspheres [37] to name but a few. Interestingly, the existence of a zero-frequency stop-band in periodically pinned plates was proposed to shield Lamb waves of very large wavelengths in [35], whereas experiments with arrays of thin elastic rods atop thin plates showed deeply subwavelength shielding and localization effects in [38]. These lead one to consider the possible implications on large-scale, i.e. meters, in terms of geophysics.

Returning to seismic waves and ground vibration, Rayleigh wave attenuation was achieved back in 1999 [39] in a marble quarry with air holes displaying kHz stop-bands; this is at a frequency range far higher than that required by the seismic application. The theoretical concept of a seismic 2D grid of inclusions in the soil interacting with a part of the earthquake signal was first created in the experiments of [40] and from hereon we too envisage a 1D or 2D phononic crystal as a 1D or 2D structured soil (natural or artificial). In 2012, with the aim of demonstrating the feasibility of the concept with field data, full-scale seismic tests were held by the Ménard company in France using a grid of vertical empty cylindrical holes with a 50 Hz source [40] that falls in the partial stop-band of the large-scale phononic crystal. This is, again, still too high for seismic applications, ideally one desires a zero-frequency stop-band structure capable of attenuating long-waves at very low frequencies. Interestingly, Miniaci *et al* [41] propose using cross-shaped, hollow and locally resonant (with rubber, steel and concrete), cylinders to attenuate both Rayleigh and bulk waves in the 1–10Hz frequency range.

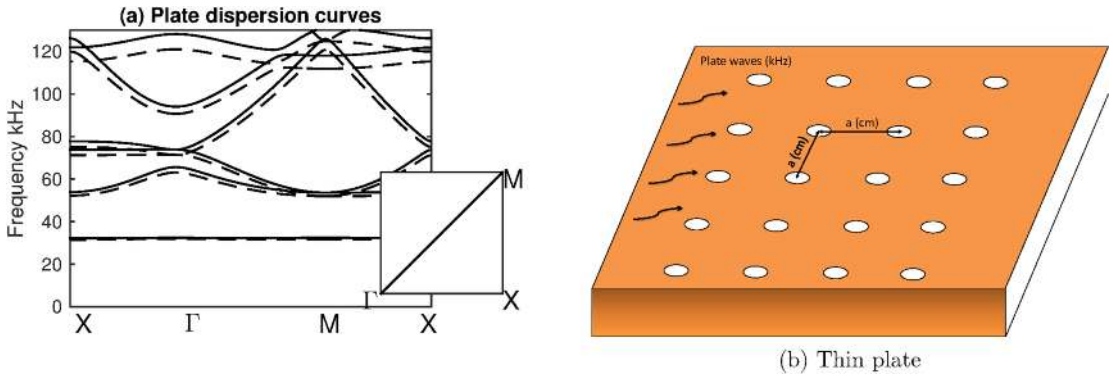

Figure 1. Clamped structured elastic plates: (a) the dispersion band diagram showing results from Kirchhoff–Love thin plate theory (solid) and full vector elastic modelling (dashed). Here $\Gamma = (0, 0)$, $M = (\pi/a, \pi/a)$ and $X = (\pi/a, 0)$ are the wavevector positions at the band edges of the irreducible Brillouin zone. (b) A schematic of the geometry for a thin clamped plate.

Unfortunately, the main drawback of this type of locally resonant structure is the difficulty in obtaining very large efficient stop bands; there is always a trade-off between the relative bandwidth and the efficiency of the attenuation, which is directly linked to the quality factor of the resonators. The frequency bandwidth of wave protection can be enlarged by considering arrays of resonant cylinders with different eigenfrequency for two-dimensional stop-bands [42], or cubic arrays of resonant spheres [43] for 3D stop-bands, but such mechanical metamaterials would be hard to implement at the civil engineering scale. Buried isochronous mechanical oscillators have been also envisaged to filter the *S* waves of earthquakes [44]. A complementary approach employed in [45, 46] is to draw upon the metamaterials literature that utilises subwavelength resonators arranged, in their case, upon the surface of an elastic half-space; this results in surface to bulk wave conversion, and surface wave filters with band-gaps but again at higher frequency than those required for seismic protection.

Identifying that the main objective of a seismic metamaterial must be to achieve a broad low-frequency stop-band, or even better a zero-frequency stop-band, we turn to the apparently, distantly connected, field of thin elastic structured plates; these are of interest in terms of flexural waves connected with the vibration of shells. The simplest model, the thin plate model of Kirchhoff and Love is well-known [47, 48] and is a fourth-order scalar partial differential equation for the vertical displacement field; this is a dramatic simplification over the full vector elastic system [49] and, for homogeneous plates, this simpler model is, in theory, valid for very thin plates with a thickness less than 1/20th of the typical wavelength [50]. None the less surprising accuracy can be obtained in structured plates, where this thickness restriction can be relaxed, and recent detailed comparison of theory and experiment [51] demonstrate that conclusions from the Kirchhoff–Love (K–L) theory carry across into thin plate modelling even at much higher frequencies where it might naively be thought to be invalid (typically in practice a plate thickness less that 1/5th of the wavelength provides good approximations for homogeneous plates); figure 1 shows dispersion curves from K–L theory alongside those of full-elasticity, both sets calculated using finite element (FE) software [52]. These are shown for a structured plate consisting of small clamped circular regions (1.5 mm radius) arranged on a square lattice of pitch 1 cm and for a 0.5 mm thick plate of duraluminium ($\rho = 2789$ kg m^{-3}, $E = 74$ GPa, $\nu = 0.33$). An important, indeed critical for our purposes here, observation, is that this system has a zero-frequency stop-band. As noted earlier there is close correspondence of full vector elastic calculations with those from K–L theory far outside the range of frequencies one might usually associate with thin plate K–L theory; the reason, as noted, in [51] is that what actually matters is not a constraint from homogeneous plates, but how the wavelengths in the periodic structured system compare to the plate thickness and they are actually large. Figure 1 takes advantage of the periodicity of the structured elastic plate, as is well-known in solid state physics [53] Bloch's theorem means that, for an infinite array, one need only consider the wavenumbers in the irreducible Brillouin zone (IBZ) which, for a square lattice, are those in the triangle ΓXM ($\Gamma = (0, 0)$, $X = (\pi/a, 0)$, $M = (\pi/a, \pi/a)$) shown as the inset to figure 1(a) and for clarity we show the frequency dependence versus wavenumbers going around the edges of the IBZ. We will exclusively use square lattices in this article and comment upon other lattice geometries in section 3 (see also figure 11).

Having successfully identified a scenario, all be it in a different situation of thin elastic plates far removed from the seismic application of thick elastic substrates, giving a zero-frequency band gap we use this to design a seismic metamaterial to have these characteristics [54]. The aim of this article is to investigate structuring soil, as shown in figure 2, to protect a building or portion of the surface. The structuration consists of columns, in a layer of soil, that are clamped to underlying bedrock; the columns are arranged in a periodic fashion. The key

(a) Side view (b) Plan view

Figure 2. The seismic metamaterial consisting of columns clamped to the bedrock surrounding the building to be protected.

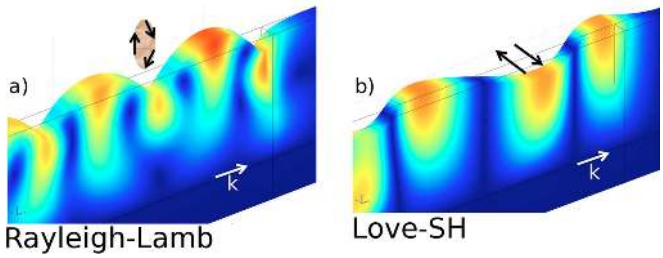

Figure 3. The polarizations and displacements of a typical Rayleigh–Lamb mode (a) and a Love-SH mode (b).

difference from all previous studies is that, motivated by thin plate calculations of figure 1 and the resultant zero frequency band gap, we consider the influence of clamping columns to the bedrock.

2. Results

We note that many seismic applications such as ground reinforcement, concern layers of softer soils overlying more solid bedrock and modern civil engineering processes allow columns to be clamped, that is, rigidly attached, to the bedrock [55]. The layers are no longer thin enough to employ K–L thin plate theory and the effect of depth (equivalently thickness of the plate) is now important. We explore the potential of seismic metamaterial devices shown in figure 2; the side view shows a structure atop a soil layer of finite thickness that overlays the bedrock; columns clamped to the bedrock puncture the soil layer and reach to the surface, or close to the surface, a top view shows the array of columns encircling the building to be protected.

For elastic waves in a finite layer, overlying a deep infinite substrate, two types of wave modes exist [48, 49]. Considering shear, SH, polarised waves one finds Love waves and these are characterised by motion concentrated in the layer and out-of-plane displacements as shown in figure 3. Love waves only exist in the layered system and not if one simply has a deep substrate alone.

An elastic substrate, of infinite depth, supports Rayleigh waves that have exponential decay with depth and whose displacements are elliptically polarised in the plane. In a finite layer depth, provided the frequency is high enough, Rayleigh waves exist as their displacement has effectively vanished at the base of the layer. As the frequency decreases the waves interact with the base and one obtains Rayleigh–Lamb modes that arise from considering an elastic waveguide. In the situations we consider we have Rayleigh-like modes that are not dominated by basal interactions and we refer to these as Rayleigh waves. Figure 3 shows the polarizations and displacements of a typical Rayleigh–Lamb mode.

We consider small strain seismicity, [56], with a rate of deformation (γ such that $\gamma \ll 10^{-4}$), in this situation the duration of seismic disturbance, for this type of earthquake, is sufficiently short to accept the validity of the hypothesis of elastic behaviour for the soil. We can therefore take realistic soil, rock and depth parameters from geophysics with the Young's modulus, $E = 3K(1 - 2\nu)$, of the soil and rock being 153 MPa and 30 GPa respectively, Poisson ratios of $\nu = 0.3$ for both and density ρ of the soil and rock being 1800 kg m^{-3} and 2500 kg m^{-3} respectively. A typical depth of soil is 15 m, which overlays bedrock of depth 5 m with effectively

rigid material beneath it (i.e. the bedrock interface is modelled with Dirichlet boundary data, which is zero displacement there).

Given the geometric and physical complexity we proceed to numerical simulations. We have three phases: the bedrock, the matrix material and the inclusions. Each of which is modelled as linear, isotropic elastic media represented by the elastic Navier equation [57] with time-harmonic motion considered at fixed frequency i.e. in the absence of any sources we take, in each phase,

$$(\lambda + \mu)\nabla(\nabla \cdot \mathbf{u}) + \mu\nabla^2\mathbf{u} = -\rho\omega^2\mathbf{u}. \tag{1}$$

There is continuity of stress and displacement across interfaces between the media and λ, μ are Lamé coefficients, ρ the density, ω the angular wave frequency and $\mathbf{u}(\mathbf{x}) = (u_1, u_2, u_3)(x_1, x_2, x_3)$ is the 3 component displacement field.

We discretize the weak form of (1) using FE methods and in particular we utilise COMSOL [52]. For band structure calculations, we take advantage of the periodicity of the system in the horizontal (x_1, x_2)-plane to consider a single elementary cell [58]. For this we use the Bloch–Floquet theorem i.e. we assume that solutions of (1) are such that

$$\mathbf{u}(\mathbf{x} + \mathbf{a}) = \mathbf{u}(\mathbf{x})\exp(\mathrm{i}\mathbf{k} \cdot \mathbf{a}) \tag{2}$$

where $\mathbf{a} = (a_1, a_2, 0)$ is the lattice vector of the 2D array of columns and $\mathbf{k} = (k_1, k_2, 0)$ is the Bloch (or momentum) wavevector in 2D reciprocal space (both $\mathbf{a}$ and $\mathbf{k}$ lie in the horizontal plane). We then construct the Bloch band spectrum, see for instance [5, 9], to obtain dispersion curves of frequency versus Bloch wavenumber. The dispersion surfaces computed are critical in guiding our understanding of the Bloch wave behaviour, we refer to [51] for structured media displaying elliptic, parabolic and hyperbolic shapes of dispersion surfaces leading to extreme elastic wave control at certain frequencies revealed by so-called high-frequency homogenization [59]. Importantly, when $|\mathbf{k}| = \sqrt{k_1^2 + k_2^2} \to 0$, the quasi-static limit of the band spectrum allows one to deduce effective properties of the periodic structure (such as anisotropy) through the slope or curvature of dispersion surfaces in the neighbourhood of Γ point [9, 60] depending upon whether they have a conical or parabolic shape. One can then interpret the effective behaviour of the low frequency Bloch waves in terms of their effective group velocity, or effective mass [61]. However, when some Dirichlet data, $\mathbf{u} = \mathbf{0}$, is set on some domain within the IBZ, corresponding to a clamped (possibly very small) inclusion, one infers from the maximum principle [9, 60] that $\mathbf{u}$ is null everywhere in the IBZ, and is not an admissible eigenfield. This seemingly minor remark has important practical consequences: it shows that a periodically constrained elastic structure has a zero-frequency stop-band, which can be used to reflect arbitrarily low frequency elastic waves. Making use of the symmetries of the periodic structure, it is common to consider the dispersion properties of Bloch waves by letting $\mathbf{k}$ vary only along the edges of the IBZ [4], and so one need only compute dispersion curves, and no longer dispersion surfaces, which greatly reduces computational effort. However, this needs to be done carefully, otherwise edges of stop-bands might be erroneously estimated [62–64].

First, simply taking into account just the finite soil layer atop the bedrock, and considering waves in this layer, leads as shown in figure 4(a), to a small zero frequency stop-band with the cut-off frequency at 2.7 Hz. This is to be expected: if one considers this layered system to be a waveguide then fixing one wall to be rigid will automatically shift the modal cut-off frequencies and no modes will propagate for extremely low frequencies. One point of note is that results, not shown, also demonstrate a weak dependence upon soil depth with the cut-off frequency rising as the depth decreases and vice versa. Although instructive, this case does not lead to the desired wide zero-frequency stop-band. Turning now to another idealised situation, that of pillars (of radius 0.3 m) that are completely rigid, and immovable all along their length, and that are buried in the bedrock, we see in figure 4(b) that an extremely wide zero-frequency stop-band stretching all the way to 30 Hz is achieved. This is unphysical as it is not possible to clamp a column all along its length, but it does demonstrate that there is potential to create a very wide band gap. The other issue is that dispersion curves are reliant upon an infinite array and for realistic systems the array will be finite.

To further motivate the importance of a zero frequency stop-band and illustrate its effect, we simulate normal incidence upon a finite array protecting a region and generate the transmission spectra. The computational domain is shown in figure 5, which consists of the clamped columns (piles) in the soil attached to bedrock with waves incident from the line source. To ensure that there is no spurious effect from the size of the computational domain elastic perfectly matched layers (PMLs) [65] are employed to prevent spurious reflections in the propagation and reflection directions. Since normal incidence is studied we will consider a single row of columns (figure 5(b)) and then use periodic conditions spanwise. We again proceed numerically in the time harmonic situation and solve the elastic Navier equation using FE methods and in particular utilise COMSOL [52] and use a line source at the surface (invariant across the domain) to initiate either Rayleigh surface waves or SH polarized waves; we use Rayleigh excitation in figure 6.

The effect of the clamped columns is most unequivocally seen by looking at the transmission spectra, that is the transmission computed at the soil/PML computational interface at the opposite side of the columns from

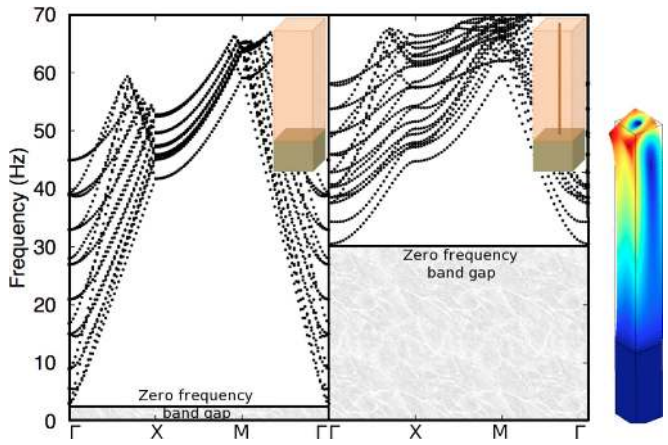

Figure 4. Dispersion curves for idealised cases: (left) clamped bedrock with no columns (centre) a clamped perfectly rigid column (i.e. with zero displacement assumed on all its boundary) of radius 0.15 m. These are shown around the edges of the irreducible Brillouin zone (see figure 1) ΓXM. The displacement is shown (right) for the mode at the band-edge for the perfectly clamped column; this is a Rayleigh mode.

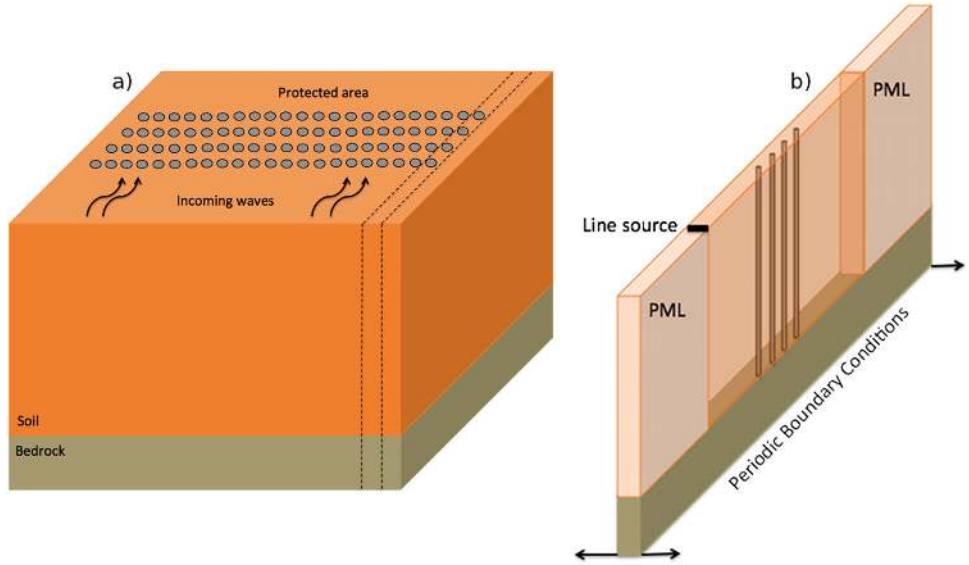

Figure 5. The computational domain for transmission spectra. (a) Waves incident upon a finite array (b) for normal incidence a reduced domain, shown by the dashed lines in (a), can be used.

the line source normalised by the amplitude of the source. The left hand panel of figure 6 shows very clearly that the fields are highly attenuated beneath the cut-off frequencies of each case, at 2.7 and 30 Hz respectively. The vertical scale is in decibels and so this represents the attenuation that would be seen, and in the clamped column case this is for just four clamped columns and is highly effective at blocking incoming waves. This is further exemplified by examining the physical fields as shown in figures 6(a), (c) for the clamped bedrock and (b), (d) for the idealised clamped, perfectly immovable, columns. The effect of the columns is clearly seen in the fields with almost perfect reflection at the frequencies illustrated.

The results above are not physically feasible as no columns can be completely fixed and rigid all along their length (i.e. zero displacement on all of its boundaries); this provides an ideal upper bound on the possible efficiency of this design, but it is highly encouraging that clamped columnar structures could, at least, achieve part of this behaviour.

We now turn to realistic designs using illustrative columnar materials and geometries. We choose two examples and treat them in detail, first cylindrical columns of steel (density 7850 kg m^{-3}, Poisson ratio 0.33), 1.2 m in diameter, in a soil layer of 15 m and bedrock of depth 5 m; the columns are buried in the bedrock to a depth of 80 cm but otherwise free to vibrate and interact with the soil and bedrock. For an infinite array placed at the vertices of a square array (of pitch 2 m) the dispersion curves are shown in figure 7(a). It is clear that this has a

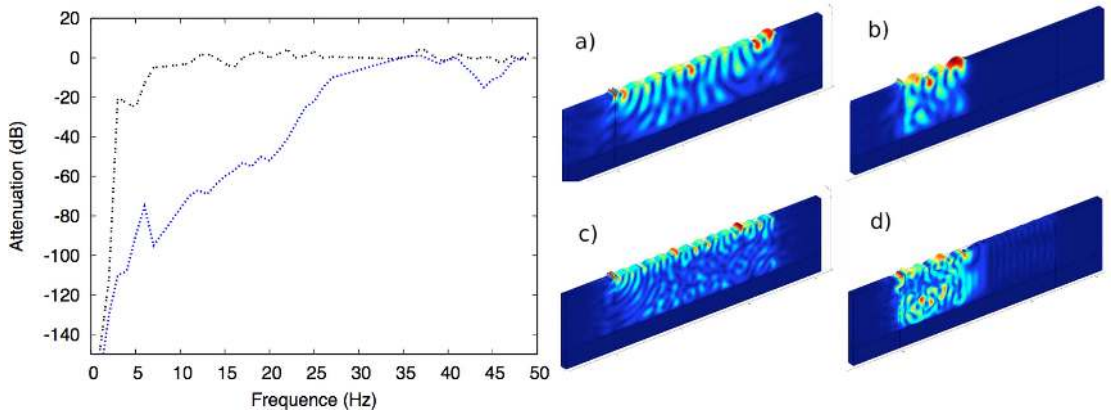

Figure 6. Idealised cases: simulations and attenuation. Panels (a), (c) show the absolute value of the vertical displacement field for the clamped bedrock respectively, (b), (d) show the field for the structured soil consisting of 4 immovable rigid columns, of radius 0.15 m, both simulations are shown for at 20 (a), (b) and 35 Hz (c), (d). The left panel shows the attenuation versus frequency with the upper curve (dashed) for soil layer with clamped bedrock and the lower curve (dotted) for the immovable rigid columns.

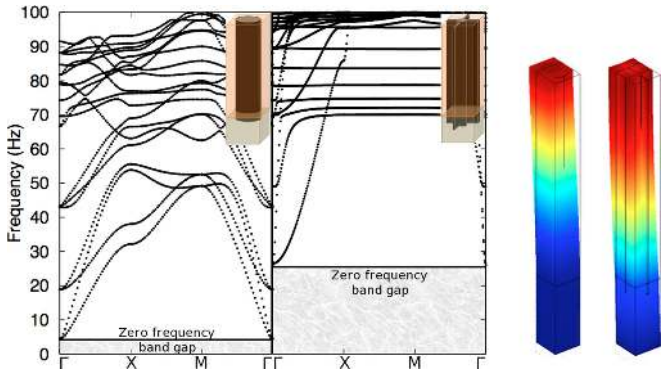

Figure 7. Dispersion curves for realistic cases: (left) steel cylindrical columns of radius 0.6 m (centre) steel columns of radius 0.3 m linked to their nearest neighbours via steel plates. Both cases have their base buried 80 cm into the bedrock. These are shown around the edges of the irreducible Brillouin zone ΓXM (see figure 1). The displacements for both cases are shown (right) for the mode at the band edge and both are shear dominated and evanescent in the bedrock.

zero-frequency stop-band up to 4.5 Hz, which is not dramatic in extent but is none the less an improvement over the unstructured soil. It is, however, far from the optimal case shown in figure 4.

It is well known in the phononic crystal community that very broad band gaps can be designed by the use of cross-shaped inclusions [66], reminiscent of lattice models [67], so we utilise this shape here and further augment this by linking the columns. We consider a cross-shaped inclusion having the same cross-sectional area as the cylinder thereby comparing inclusions that have the same filling fraction. In this second configuration we take a cylindrical column of radius 0.2 m and each column is then linked to its nearest neighbours by struts (long steel plates of 0.2 m in thickness), see figure 7(b), and this also gives the columns a structural link to its neighbours. This additional reinforcement then leads to a dramatic enhancement in the protected frequency range, which is now up to 26 Hz. The dispersion curves of figure 7 are for an infinite array and do not reveal the potential efficiency of the design, as for this we need the transmission spectra.

We consider both shear wave and Rayleigh wave incidence, as they have different character. Shear wave incidence is illustrated in figure 8 that shows the attenuation of the clamped cylinders and the clamped cross-shaped inclusions; the latter clearly perform much better and the attenuation is strongly enhanced below 26 Hz. Notably this performance is for normal incidence upon a finite array only four columns deep, and improves further if the number of columns is increased. Movies constructed using the time harmonic solutions to show the time evolution of an incoming wave incident upon the columns are shown in the supplementary material (available online at stacks.iop.org/NJP/19/063022/mmedia). As an aside in figure 8 there is a dip in the transmission spectra for the clamped cylindrical columns at approximately 40 Hz, which is due to the polarisation of the source and its interaction with the phononic crystal; this can be identified in figure 13(A) when taking into account the polarization state of shear waves.

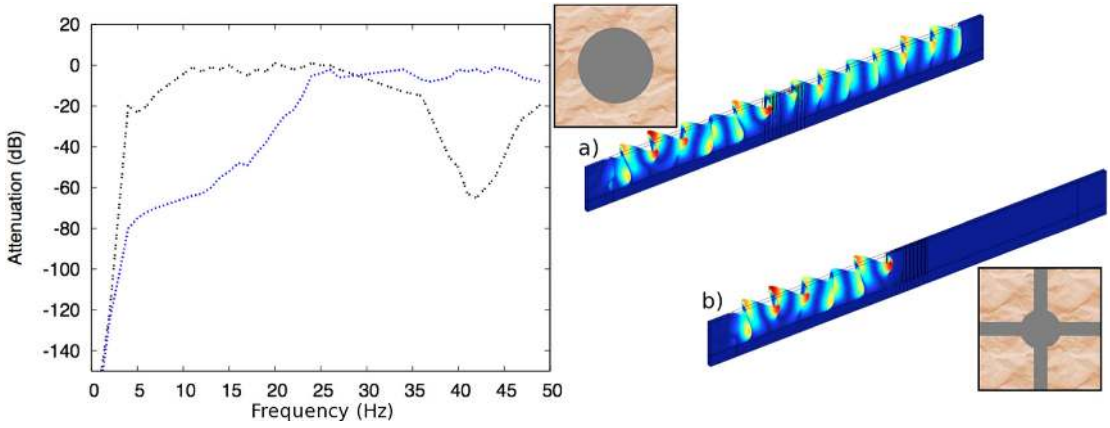

Figure 8. Attenuation (in dB) of incoming shear waves versus frequency (in Hz) through an array as in figure 5 with 4 rows of clamped cylindrical inclusions of radius 0.6 m (upper black curve) and clamped cross-shaped inclusions (lower blue curve). The absolute value of the vertical displacement at 13 Hz for (a) the steel column and (b) a column augmented by attachments to its neighbours; the geometries, which share the same filling fraction, are shown as insets. (Movies demonstrating this behaviour are in the associated Supplementary material as pile-13 Hz.avi croix-13 Hz.avi for (a) and (b) respectively.)

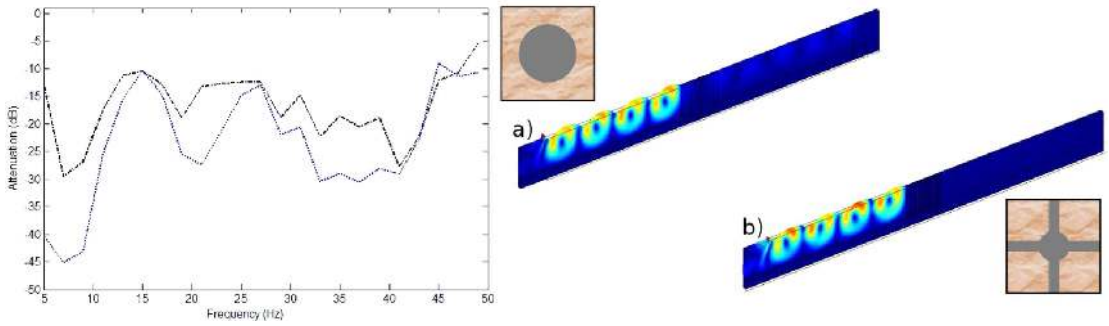

Figure 9. Attenuation (in dB) of incoming Rayleigh waves versus frequency (in Hz) through an array as in figure 5 with 10 rows of clamped cylindrical inclusions of radius 0.6 m (upper curve) and clamped cross-shaped inclusions (lower curve). The absolute value of the vertical displacement at 9 Hz for (a) the steel column and (b) a column augmented by attachments to its neighbours; the geometries, which share the same filling fraction, are shown as insets.

Rayleigh wave incidence is illustrated in figure 9 showing again attenuation of the clamped cylinders and the clamped cross-shaped inclusions and the associated displacement fields. The attenuation is not as dramatic as for shear waves due to the stronger coupling of Rayleigh waves into the structure and the finite structure as a whole can vibrate, i.e. the signal at 15 Hz, none the less strong attenuation is achieved for low frequencies.

We now address the issue of whether there is an optimal filling fraction. In figure 10 we show the upper extent of the zero frequency band-gap for the cross-like inclusions and cylindrical inclusions. In the latter case the upper extent increases monotonically as the filling fraction (also called the soil substitution in the civil engineering literature) increases, as one would expect. For the cross-like inclusion there is a non-monotonic behaviour, all be it very gradual, with a maximum for a filling faction of around 0.6. In practical terms, a soil substitution rate beyond 10%–20% is quite substantial in civil engineering, and in practice the smaller filling fractions are more relevant.

It is natural, of course, given that we have presented in detail a design on a square lattice to consider whether changing the underlying lattice structure to another Bravais lattice creates fundamental changes. It does not, it alters the detail of the extent of the zero frequency band gap but not the physics behind this. As a further illustration we show, in figure 11, the dispersion curves for the steel columns (radius 0.3 m and buried 80 cm in the bedrock) placed on a honeycomb lattice with plate attachments along the honeycomb. Again one notes an extensive zero frequency bandgap extending up to 20 Hz, thus there is unfortunately no specific advantage of using a honeycomb, instead of square, array. Similarly we also considered hexagonal arrays with a band-gap extending to 18 Hz and it is clear that unlike the case of phononic crystals or locally resonant materials, the hexagonal lattice is less efficient compared to the honeycomb or square lattices.

A key point of the design, further emphasised in [68], is the burying of columns in the bedrock and connectivity between columns and to demonstrate how important this is we consider an array of horizontal steel

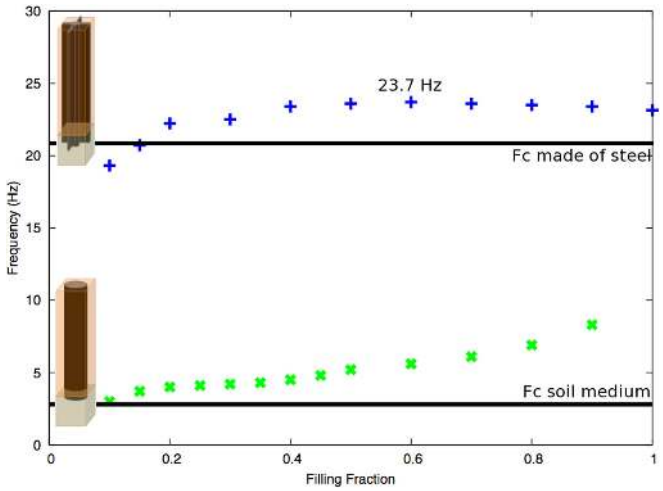

Figure 10. The upper extent of the zero frequency band-gap versus filling fraction (i.e. soil substitution rate) for the clamped cylindrical and cross-like inclusions. Note the upper curve is non-monotonic and these are modes at the band edge, which have shear-like character.

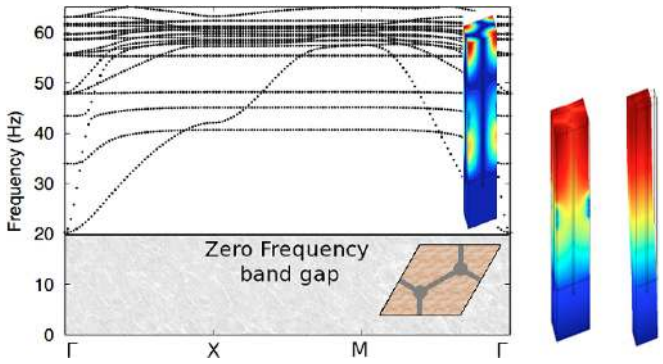

Figure 11. Dispersion curves for steel columns of radius 0.3 m arranged on a honeycomb lattice of pitch $2\sqrt{3}$ to maintain 2 m spacing between adjacent columns and attached by steel plates along the honeycomb lattice. Inset we show the eigenmode of the lowest flat band showing how the energy is stored between the plates. We also show the total displacement of the eigenmode at the cut-off frequency for the honeycomb lattice (19.6 Hz) and hexagonal lattice (18.3 Hz); both are shear dominated modes.

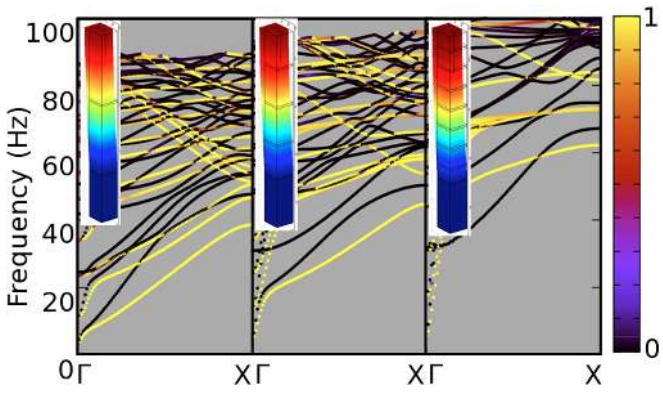

Figure 12. The dispersion curves along ΓX for a vertical steel column of radius 0.3 m piercing horizontal steel plates of thickness 0.2 m. From left to right we start with a single plate at depth 7.5 m splitting the soil layer in half with then 3 and 7 equally spaced plates in the other two panels. The colours of the bands show the amount of polarization, p_2, (3), along the propagation direction (x_2 axis) with yellow being shear dominated; thus the mode at the band-edge has the character of a shear-like mode.

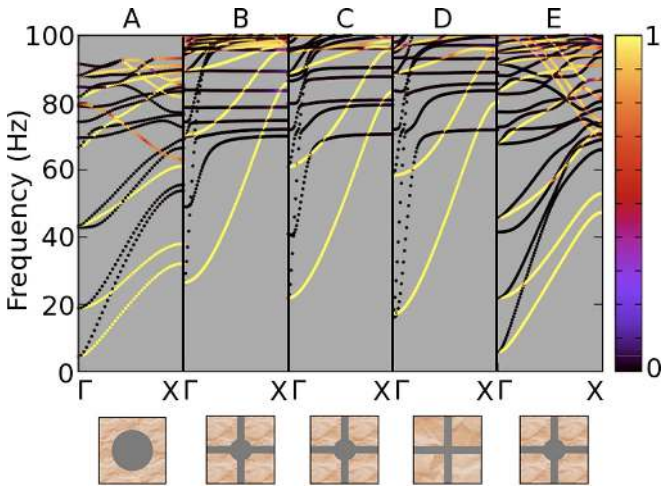

Figure 13. Dispersion curves in $X\Gamma$ for 5 cases. (A), is the steel column of figure 6(a) buried 80 cm in bedrock, (B), is the steel column joined to its neighbours in a square lattice, buried 80 cm of figure 6(b). Panels (C) and (D) are not buried in the rock and merely are joined at the soil/bedrock interface to the bedrock and then have the central steel column absent respectively. (E) Shows the effect of decoupling the joining plates at the edges of the periodic cell. For clarity the cross-section of the cell is shown beneath each case. The colours of the bands show the amount of polarization, p_2, (3), along the propagation direction (x_2 axis) with yellow being shear dominated; thus the mode at the band-edge has the character of a shear-like mode.

plates of thickness 0.2 m that splits the soil layer into a laminate structure and a column of radius 0.3 m; the band diagrams for this structure are shown in figure 12 that also shows the polarization p_2 (along x_2) defined as

$$p_2^2 = \frac{1}{V}\int_{-a_1}^{a_1}\int_{-a_2}^{a_2}\int_0^h \frac{|u_2|^2}{|u_1|^2 + |u_2|^2 + |u_3|^2}\mathrm{d}x_1\mathrm{d}x_2\mathrm{d}x_3, \tag{3}$$

where the triple integral is over the periodic cell $[-a_1, a_1] \times [-a_2, a_2] \times [0, h]$ with $a_1 = a_2 = 1$ m the array pitch, $h = 15$ m the soil depth and V the volume of the cell. Here there is no zero frequency band gap with the dispersion curves always passing through the origin, however there are some interesting features observable in this diagram. For instance, there are pronounced changes of curvature in the lower bands that may be of interest and as one increases the lamination the regions of wavenumber space for which there is propagation shrink.

Finally, we investigate the sensitivity of the upper-extent of the zero-frequency band gap to attachment in the bedrock and to modifying the square lattice structure of a steel rod attached to its neighbours by steel plates. We do this in figure 13 and show the dispersion curves only in the ΓX direction, that is for normal propagation to an array, and consider 5 cases: A, is the steel column of radius 0.6 m of figure 7(a) buried 80 cm in bedrock showing a small zero-frequency band-gap, (B), is the reference case of the steel column of radius 0.3 m joined to its neighbours in a square lattice, buried 80 cm of figure 7(b) and sharing the same filling fraction as A. Panels (C) and (D) are not buried in the rock and merely are joined at the soil/bedrock interface to the bedrock and then have the central steel column absent respectively; the upper extent of the band-gap decreases. (E) goes one stage further and decouples the joining plates at the edges of the periodic cell and then the band-gap width decreases dramatically. It is clear that the combination of having the steel column, buried in the bedrock, and the coupling of each column to its neighbours via the steel plates is essential to obtain the broad ultra-low frequency stop-bands.

3. Discussion

In geotechnics, so-called composite soils made of inclusions inserted in a matrix of soil are mainly developed using a pseudo-static analysis; the dynamic loading is converted into an equivalent static loading and the objective is to obtain a higher value of Youngs modulus or shear modulus G (or μ) in order to reduce the deformation of the soil-deep foundation system [69, 70]. Homogenization techniques have been also applied to composite soils [71, 72] and recently developed for dynamic loading [73]. The emerging field of seismic metamaterials, based on wave physics, enables us to revisit several longstanding problems of earthquake protection from this fully dynamic point of view.

In this vein, we have considered here how one could use these wave physics-based ideas to protect specific areas from low-frequency vibration. We have demonstrated, conclusively, that it is possible to design realistic seismic metamaterial devices, in the sense of the structures that form the material being subwavelength and in the limit of small strains such that we have linear elastic conditions. The desired performance is achieved by creating zero-frequency stop-bands using clamping of columns to underlying bedrock. Clearly the challenge is

now to build such structures in the spirit of [40] and we anticipate that these results will motivate large-scale experiments to verify this since there are potential applications in seismic defence structures [68]. It is notable that zero-frequency stop-bands will arise in other areas of physics whenever periodic arrays of inclusions have zero field, i.e. Dirichlet data, on their boundary see for instance, [74], in the context of electromagnetic waves or [75] for clamped inclusions in full vector elasticity. One can anticipate this, following [74] any Floquet–Bloch eigenvalue problem involving inclusions with zero Dirichlet data on part of their boundary, will display zero frequency stop-bands, since the existence of an eigenfield associated with a zero frequency would imply by the maximum principle that the eigenfield is null everywhere. Therefore, any wave (electromagnetic, acoustic, hydrodynamic, elastodynamic) will be prohibited to propagate within a periodic structure at very low frequencies provided inclusions can be modelled with zero Dirichlet data (e.g. infinite conducting inclusions in the case of electromagnetics and clamped inclusions in the case of elastodynamics).

Although we have concentrated here on the lowest dispersion curve, at high frequencies, the dispersion curves and asymptotics based around generating dynamic effective media [75–77] suggest that interesting features will also occur. These include ultra-directivity whereby a periodically pinned plate behaves like an extremely anisotropic effective medium at frequencies associated with flat bands on dispersion diagrams [51].

Finally, we note that we assumed a linear elastic model for soil and columns of concrete, however, the former has visco-elastic features, that could also be implemented e.g. via a Kelvin–Voigt contact condition at the soil-column interfaces. Intuitively, we expect that such a model would reduce the local resonances, and the extremely high damping seen in figures 5 and 8 around certain frequencies, would be less pronounced.

Acknowledgments

RC thanks the EPSRC for their support through research grants EP/I018948/1, EP/L024926/1, EP/J009636/1. SG and YA are thankful for an ERC starting grant (ANAMORPHISM) that facilitated the collaboration with Imperial College London.

We also thank A Diatta for his help in the implementation of Cartesian PMLs in elasticity.

Appendix. Material values and parameters

For clarity and convenience we summarize the values used in the text.

Parameters	Soil	Bedrock	Steel columns	Steel plates
Depth	15 m	5 m	15 m	
Square pitch			2 m	
Honeycomb pitch			$2\sqrt{3}$ m	
Plate thickness				0.2 m
column radius			0.15 m (figures 3(b), 4, 5(b), (d)) 0.3 m (figures 6(b), 7(b), 8(b), 10, 11, 12(b), (c), (e)) 0.6 m (figures 6(a), 12(a))	
Young modulus E (GPa)	0.153	30	200	200
Poisson's ratio ν	0.3	0.3	0.33	0.33
Density ρ (kg m^{-3})	1800	2500	7850	7850

References

[1] Reitherman R 2012 *Earthquakes and Engineers: An International History* (Reston, VA: ASCE Press)
[2] Brûlé S, Javelaud E and Marchand M 2012 Chimneys health monitoring during a nearby heavy dynamic compaction site *J. Nat. Géotechn. Géol. l'Ingén.* **2** 919–26
[3] Chopra A 2012 *Dynamics of Structures. Theory and Applications to Earthquake Engineering* (London: Prentice-Hall)
[4] Joannopoulos J D, Johnson S G, Winn J N and Meade R D 2008 *Photonic Crystals, Molding the Flow of Light* 2nd edn (Princeton, NJ: Princeton University Press)
[5] Zolla F, Renversez G, Nicolet A, Kuhlmey B, Guenneau S and Felbacq D 2005 *Foundations of Photonic Crystal Fibres* (London: Imperial College Press)
[6] John S 1987 Strong localization of photons in certain disordered dielectric superlattices *Phys. Rev. Lett.* **58** 2486–9
[7] Yablonovitch E 1987 Inhibited spontaneous emission in solid-state physics and electronics *Phys. Rev. Lett.* **58** 2059

[8] Wilcox C 1978 Theory of Bloch waves *J. Anal. Math.* **33** 146–67
[9] Conca C, Planchard J and Vanninathan M 1995 *Fluids and Periodic Structures* (*Research in Applied Mathematics*) (Paris: Masson)
[10] Gazalet J, Dupont S, Kastelik J C, Rolland Q and Djafari-Rouhani B 2013 A tutorial survey on waves propagating in periodic media: electronic, photonic and phononic crystals. Perception of the Bloch theorem in both real and fourier domains *Wave Motion* **50** 619–54
[11] Chen A L and Wang Y S 2007 Study on band gaps of elastic waves propagating in one-dimensional disordered phononic crystals *Physica* B **392** 369–78
[12] Figotin A and Vitebskiy I 2006 Slow light in photonic crystals *Waves Random Complex Media* **16** 293–392
[13] Pendry J B 2000 Negative refraction makes a perfect lens *Phys. Rev. Lett.* **85** 3966–9
[14] Ramakrishna S A 2005 Physics of negative refractive index materials *Rep. Prog. Phys.* **68** 449–521
[15] Iorch I V, Mukhin I S, Shadrivov I V, Belov P A and Kivshar Y S 2013 Hyperbolic metamaterials based on multilayer graphene structures *Phys. Rev.* B **87** 075416
[16] Pendry J B, Schurig D and Smith D R 2006 Controlling electromagnetic fields *Science* **312** 1780–2
[17] Leonhardt U 2006 Optical conformal mapping *Science* **312** 1777–80
[18] Economou E N and Sigalas M M 1993 Classical wave propagation in periodic structures: cermet versus network topology *Phys. Rev.* B **48** 13434–8
[19] Martinez-Sala R, Sancho J, Sanchez J V, Gomez V, Linares J and Meseguer F 1995 Sound attenuation by sculpture *Nature* **378** 241
[20] Hu X and Chan C T 2005 Refraction of water waves by periodic cylinder arrays *Phys. Rev. Lett.* **95** 154501
[21] Farhat M, Enoch S, Guenneau S and Movchan A B 2008 Broadband cylindrical acoustic cloak for linear surface waves in a fluid *Phys. Rev. Lett.* **101** 1345011
[22] Dupont G, Kimmoun O, Molin B, Guenneau S and Enoch S 2015 Numerical and experimental study of an invisibility carpet in a water channel *Phys. Rev.* E **91** 023010
[23] Berraquero C P, Maurel A, Petitjeans P and Pagneux V 2013 Experimental realization of a water-wave metamaterial shifter *Phys. Rev.* E **88** 051002(R)
[24] Evans D V and Porter R 2007 Penetration of flexural waves through a periodically constrained thin elastic plate floating *in vacuo* and floating on water *J. Eng. Math.* **58** 317–37
[25] Colquitt D J, Craster R V, Antonakakis T and Guenneau S 2015 Rayleigh–Bloch waves along elastic diffraction gratings *Proc. R. Soc.* A **471** 20140465
[26] Maier S 2010 *Plasmonics: Fundamentals and Applications* (London: Springer)
[27] Pendry J B, Martin-Moreno L and Garcia-Vidal F J 2004 Mimicking surface plasmons with structured surfaces *Science* **305** 847–8
[28] Benchabane S, Khelif A, Rauch J Y, Robert L and Laude V 2006 Evidence for complete surface wave band gap in a piezoelectric phononic crystal *Phys. Rev.* E **73** 065601
[29] Benchabane S, Gaiffe O, Ulliac G, Salut R, Achaoui Y and Laude V 2011 Observation of surface-guided waves in holey hypersonic phononic crystal *Appl. Phys. Lett.* **98** 171908
[30] Khelif A, Achaoui Y, Benchabane S, Laude V and Aoubiza B 2010 Locally resonant surface acoustic wave band gaps in a two-dimensional phononic crystal of pillars on a surface *Phys. Rev.* B **81** 214303
[31] Achaoui Y, Khelif A, Benchabane S, Robert L and Laude V 2011 Experimental observation of locally-resonant and bragg band gaps for surface guided waves in a phononic crystal of pillars *Phys. Rev.* B **10** 104201
[32] Al-Lethawe M A, Addouche M, Khelif A and Guenneau S 2012 All-angle negative refraction for surface acoustic waves in pillar-based two-dimensional phononic structures *New J. Phys.* **14** 123030
[33] Pierre J, Boyko O, Belliard L, Vasseur J O and Bonello B 2010 Negative refraction of zero order flexural lamb waves through a two-dimensional phononic crystal *Appl. Phys. Lett.* **97** 121919
[34] Dubois M, Farhat M, Bossy E, Enoch S, Guenneau S and Sebbah P 2013 Flat lens for pulse focusing of elastic waves in thin plates *Appl. Phys. Lett.* **103** 071915
[35] Antonakakis T, Craster R V and Guenneau S 2014 Moulding and shielding flexural waves in elastic plates *Europhys. Lett.* **105** 54004
[36] Graczykowski B, Sledzinska M, Alzina F, Gomis-Bresco J, Reparaz J S, Wagner M R and Torres C M S 2015 Phonon dispersion in hypersonic two-dimensional phononic crystal membranes *Phys. Rev.* B **91** 075414
[37] Boechler N, Eliason J K, Kumar A, Maznev A A, Nelson K A and Fang N 2013 Interaction of a contact resonance of microspheres with surface acoustic waves *Phys. Rev. Lett.* **111** 036103
[38] Colombi A, Roux P and Rupin M 2014 Sub-wavelength energy trapping of elastic waves in a meta-material *J. Acoust. Soc. Am.* **136** 104201
[39] Meseguer F, Holgado M, Caballero D, Benaches N, Sanchez-Dehesa J, Lopez C and Llinares J 1999 Rayleigh-wave attenuation by a semi-infinite two-dimensional elastic-band-gap crystal *Phys. Rev.* B **59** 12169
[40] Brûlé S, Javelaud E H, Enoch S and Guenneau S 2014 Experiments on seismic metamaterials: molding surface waves *Phys. Rev. Lett.* **112** 133901
[41] Miniaci M, Krushynska A, Bosia F and Pugno N M 2016 Large scale mechanical metamaterials as seismic shields *New J. Phys.* **18** 083041
[42] Krodel S, Thome N and Daraio C 2015 Wide band-gap seismic metastructures *Ext. Mech. Lett.* **4** 111–7
[43] Achaoui Y, Ungureanu B, Enoch S, Brule S and Guenneau S 2016 Seismic waves damping with arrays of inertial resonators *Ext. Mech. Lett.* **8** 30–7
[44] Finocchio G, Casablanca O, Ricciardi G, Alibrandi U, Garesci F, Chiappini M and Azzerboni B 2014 Seismic metamaterials based on isochronous mechanical oscillators *Appl. Phys. Lett.* **104** 191903
[45] Colombi A, Roux P, Guenneau S, Gueguen P and Craster R V 2016 Forests as a natural seismic metamaterial: Rayleigh wave bandgaps induced by local resonances *Sci. Rep.* **6** 19238
[46] Colombi A, Colquitt D, Roux P, Guenneau S and Craster R V 2016 A seismic metamaterial: the resonant metawedge *Sci. Rep.* **6** 27717
[47] Landau L D and Lifshitz E M 1970 *Theory of Elasticity* 2nd edn (Oxford: Pergamon)
[48] Graff K F 1975 *Wave Motion in Elastic Solids* (Oxford: Oxford University Press)
[49] Achenbach J D 1984 *Wave Propagation in Elastic Solids* (Amsterdam: North-Holland)
[50] Rose L R F and Wang C H 2004 Mindlin plate theory for damage detection: source solutions *J. Acoust. Soc. Am.* **116** 154–71
[51] Lefebvre G, Antonakakis T, Achaoui Y, Craster R V, Guenneau S and Sebbah P 2016 Unveiling extreme anisotropy in elastic structured media arXiv:1610.04884
[52] COMSOL User's Guide version 5.2, 2016 http://comsol.com/
[53] Kittel C 1996 *Introduction to Solid State Physics* 7th edn (New York: Wiley)
[54] Colquitt D, Colombi A, Craster R V, Roux P and Guenneau S 2016 Seismic metasurfaces: sub-wavelength resonators and Rayleigh wave interaction *J. Mech. Phys. Sol.* **99** 379–93

[55] Brûlé S, Enoch S, Guenneau S and Craster R V 2017 Seismic metamaterials: controlling surface Rayleigh waves using analogies with electromagnetic metamaterials *Handbook of Metamaterials* (Singapore: World Scientific) in press
[56] Semblat J F and Pecker A 2009 *Waves and Vibrations in Soils: Earthquakes, Traffic, Shocks, Construction Works* (Pavia: IUSS Press)
[57] Ciarlet P G 1997 *Mathematical Elasticity. Volume II: Theory of Plates* (Amsterdam: North-Holland)
[58] Nicolet A, Guenneau S, Geuzaine C and Zolla F 2004 Modeling of electromagnetic waves in periodic media with finite elements *J. Comput. Appl. Math.* **168** 321–9
[59] Craster R V, Kaplunov J and Pichugin A V 2010 High frequency homogenization for periodic media *Proc. R. Soc.* A **466** 2341–62
[60] Bensoussan A, Lions J L and Papanicolaou G 1978 *Asymptotic Analysis for Periodic Structures* (Amsterdam: North-Holland)
[61] Guenneau S, Poulton C G and Movchan A B 2003 Oblique propagation of electromagnetic and elastodynamic waves for an array of cylindrical fibres *Proc. R. Soc.* A **459** 2215–63
[62] Harrison J M, Kuchment P, Sobolev A and Winn B 2007 On occurrence of spectral edges for periodic operators inside the Brillouin zone *J. Phys. A: Math. Theor.* **40** 7597–618
[63] Craster R V, Antonakakis T, Makwana M and Guenneau S 2012 Dangers of using the edges of the Brillouin zone *Phys. Rev.* B **86** 115130
[64] Brule Y, Gralak B and Demesy G 2016 Calculation and analysis of the complex band structure of dispersive and dissipative two-dimensional photonic crystals *J. Opt. Soc. Am.* B **33** 691
[65] Diatta A, Kadic M, Wegener M and Guenneau S 2016 Scattering problems in elastodynamics *Phys. Rev.* B **94** 100105
[66] Wang Y-F, Wang Y-S and Su X-X 2011 Large bandgaps of two-dimensional phononic crystals with cross-like holes *J. Appl. Phys.* **110** 113520
[67] Martinsson P G and Movchan A B 2003 Vibrations of lattice structures and phononic band gaps *Q. J. Mech. Appl. Math.* **56** 45–64
[68] Achaoui Y, Antonakakis T, Brulé S, Craster R, Enoch S and Guenneau S 2016 Seismic defence structures *UK Patent* GB 1617808.9
[69] AFPS and CFMS 2012 *Procédés D'amélioration Et De Renforcement De Sols sous Action Sismique:Guide technique* (Paris: Presses des Ponts)
[70] Pecker A and Teyssandier P 2009 Conception parasismique du pont de rion-antirion *19ème Congrès Franais de Mécanique (Marseille, 24–28 August)*
[71] De Buhan P 1986 Approche fondamentale du calcul à la rupture des ouvrages en sols renforcés *Thèse de Doctorat dEtat* Université Paris Est, Paris
[72] Guéguin M 2014 Approche par une méthode d'homogénéisation du comportement des ouvrages en sols renforcés par colonnes ou tranchées *Thèse de Troisième Cycle* Université Paris Est, Paris
[73] Nguyen V 2014 Analyse sismique des ouvrages renforcés par inclusions rigides à l'aide dune modélisation multiphasique *Thèse de Troisième Cycle* Université Paris Est, Paris
[74] Poulton C G, Botten L C, McPhedran R C, Nicorovici N A and Movchan A B 2001 Non-commuting limits in electromagnetic scattering: an asymptotic analysis for an array of highly conducting inclusions *SIAM J. Appl. Math.* **61** 1706–30
[75] Antonakakis T, Craster R V and Guenneau S 2014 Homogenisation for elastic photonic crystals and dynamic anisotropy *J. Mech. Phys. Sol.* **71** 84–96
[76] Auriault J L and Boutin C 2012 Long wavelength inner-resonance cut-off frequencies in elastic composite materials *Int. J. Sol. Struct.* **49** 3269–81
[77] Boutin C, Rallu A and Hans S 2014 Large scale modulation of high frequency waves in periodic elastic composites *J. Mech. Phys. Sol.* **70** 362–81